2012

The helium-rich subdwar CPD-20d1123: a post-common-envelope binary evolving on to the extended horizontal branch

Vincent M Woolf, *University of Nebraska at Omaha*

Monthly Notices
of the
ROYAL ASTRONOMICAL SOCIETY

Mon. Not. R. Astron. Soc. **423,** 3031–3038 (2012) doi:10.1111/j.1365-2966.2012.21012.x

The helium-rich subdwarf CPD−20°1123: a post-common-envelope binary evolving on to the extended horizontal branch

N. Naslim,[1⋆] S. Geier,[2⋆] C. S. Jeffery,[1⋆] N. T. Behara,[1,3] V. M. Woolf[4] and L. Classen[2]

[1]*Armagh Observatory, College Hill, Armagh BT61 9DG*
[2]*Dr Karl Remeis-Sternwarte & ECAP, Astronomisches Institüt, Friedrich-Alexander Universität Erlangen-Nürnberg, Sternwartstr. 7, D 96049 Bamberg, Germany*
[3]*Institut d'Astronomie et d'Astrophysique, Université Libre de Bruxelles, Belgium*
[4]*Physics Department, University of Nebraska at Omaha, Omaha, NE 68182-0266, USA*

Accepted 2012 March 29. Received 2012 March 24; in original form 2012 February 15

ABSTRACT

Subluminous B stars come in a variety of flavours including single stars, close and wide binaries, and pulsating and non-pulsating variables. A majority have helium-poor surfaces (helium by number $n_{\rm He} < 1$ per cent), whilst a minority have extremely helium rich surfaces ($n_{\rm He} > 90$ per cent). A small number have an intermediate surface helium abundance (≈10–30 per cent), accompanied by peculiar abundances of other elements. The questions posed are (i) whether these abundance peculiarities are associated with radiatively driven and time-dependent stratification of elements within the photosphere as the star evolves from a helium-enriched progenitor to become a normal helium-poor sdB star and (ii) whether these phenomena occur only in single sdB stars or are also associated with sdB stars in binaries.

We present a fine analysis of the bright intermediate helium sdB star CPD−20°1123 (Albus 1) which shows it to be cool, for a hot subdwarf, with $T_{\rm eff} \approx 23\,000$ K and with a surface helium abundance ≈17 per cent by number. Other elements do not show extraordinary anomalies; in common with majority sdB stars, carbon and oxygen are substantially depleted, whilst nitrogen is enriched. Magnesium through sulphur appear to be depleted by ≈0.5 dex, but chlorine and argon are substantially enhanced.

We also present a series of radial velocity measurements which show the star to be a close binary with an orbital period of 2.3 d, suggesting it to be a post-common-envelope system.

The discovery of an intermediate helium rich sdB star in a close binary in addition to known and apparently single exemplars supports the view that these are very young sdB stars in which radiatively driven stratification of the photosphere is incomplete.

Key words: stars: abundances – binaries: general – stars: chemically peculiar – stars: evolution – stars: horizontal branch – subdwarf.

1 INTRODUCTION

Subdwarf B stars are low-mass core helium burning stars with extremely thin hydrogen envelopes. They behave as helium main-sequence stars of roughly half a solar mass. Their atmospheres are generally helium deficient; radiative levitation and gravitational settling combine to make helium sink below the hydrogen-rich surface (Heber 1986) to deplete other light elements and to enhance abundances of heavy elements in the photosphere (O'Toole & Heber 2006).

However, almost 10 per cent of the total subdwarf population comprise stars with helium-rich atmospheres (Green, Schmidt & Liebert 1986; Ahmad & Jeffery 2006). They have been variously classified as sdOB, sdOC and sdOD (Green et al. 1986) stars, but more recently as He-sdB and He-sdO stars (Moehler et al. 1990; Ahmad & Jeffery 2004). Their optical spectra are characterized by strong He I (He-sdB) and He II (He-sdO) lines. The helium-rich subdwarfs (He-sds) may be further divided into *extremely* helium rich stars (≈95 per cent of He-sds having surface helium abundances >80 per cent by number) and a small number of *intermediate* helium rich stars [≈5 per cent of He-sds, having surface helium

⋆E-mail: nas@arm.ac.uk (NN); stephan.geier@sternwarte.uni-erlangen.de (SG); csj@arm.ac.uk (CSJ)

abundances >5 per cent and <80 per cent by number (Naslim et al. 2010)]. Whilst the extreme He-sdB stars may well be the product of double helium white dwarf mergers (Zhang & Jeffery 2012), the intermediate He-sdB stars are more difficult to explain and include stars as diverse as the prototype JL 87 (Ahmad et al. 2007), the extremely peculiar LS IV−14°116 (Naslim et al. 2011) and also UVO 0512–08 and PG 0909+276 (Edelmann 2003).

CPD−20°1123 (Albus 1 or TYC 5940 962 1) is one of the brightest known He-sdB stars with a V magnitude 11.75 ± 0.07 (Vennes, Kawka & Smith 2007). This object was first reported by Gill & Kapteyn (1896) with a photographic magnitude 10.6. Caballero & Solano (2007) suggested it might be a hot white dwarf or possibly a hot subdwarf at a distance $d \approx 40$ pc. Vennes et al. (2007) classified it as a bright helium-rich subdwarf B star with $T_{\rm eff} = 19\,800$ K and $\log g = 4.55$ using low-resolution optical spectra.

This paper reports a detailed atmospheric study using a high-resolution optical spectrum which confirms CPD−20°1123 to be an *intermediate* helium rich sdB star. It also reports a radial velocity (RV) study which shows CPD−20°1123 to be the first such star to be also a single-lined spectroscopic binary. It will be argued that these results may have profound implications for understanding the origin of *normal* sdB stars.

2 OBSERVATIONS AND RADIAL VELOCITIES

Service-mode observations of CPD−20°1123 were made at the Australian Astronomical Telescope (AAT) with the University College London Echelle Spectrograph (UCLES) on 2010 January 14 using the 31 lines mm^{-1} grating to give a wavelength coverage of λ = 3820–5230 Å. A series of six high-resolution optical spectra were made in very poor seeing (>3 arcsec) with 1-arcsec slit delivering a resolution $R \simeq 45\,000$, and a total exposure time of 9000 s. The observations were combined, flat-fielded, sky subtracted and wavelength calibrated. The individual orders were merged and the final spectrum was normalized.

The AAT/UCLES spectrum displays strong C II, N II, Mg II, Al III, Si II, Si III, P III, S II and S III lines, together with Ar II, Cl II and Fe III lines. Unlike most other He-sdB stars, the optical spectrum shows relatively strong hydrogen Balmer lines along with strong Stark-broadened He I 4471, 4922, 4388 lines. This places the star in the list of hot subdwarfs with intermediate helium abundance, alongside JL 87 (Ahmad et al. 2007) and LS IV−14°116 (Naslim et al. 2011), but the absence of He II 4686 Å suggests a much lower effective temperature. The lines due to chlorine, argon and iron-group elements have not been observed in any other He-sdB star (Naslim et al. 2010).

15 medium-resolution spectra were obtained with the ESO Multi-Mode Instrument (EMMI) spectrograph ($R \simeq 3400$, λ = 3880–4380 Å) mounted at the European Southern Observatory's (ESO's) New Technology Telescope (NTT) in 2008 January. Reduction was done with the ESO MIDAS package. The RVs were measured by fitting a set of functions to the hydrogen Balmer and neutral helium lines using the FITSB2 routine (Napiwotzki et al. 2004). Gaussians were used to match the line cores, Lorentzians for the line wings and polynomials to match the continuum. The RV of the star was found to be variable on a time-scale of days. The statistical 1σ errors of the single measurements ranged from 5 to 7 km s^{-1}. In order to derive the systematic uncertainties we calculated the standard deviation of eight RVs from spectra taken consecutively during the last night within only ≃0.13 d assuming that the orbital period is much longer than that. This standard deviation of 8 km s^{-1} was then adopted as the uncertainty for all RVs.

Table 1. RVs of CPD−20°1123.

Mid-HJD	RV (km s^{-1})	Instrument
245 4476.673 64	−31.8 ± 8.0	EMMI
245 4476.720 33	−32.0 ± 8.0	
245 4477.667 01	16.3 ± 8.0	
245 4477.835 49	27.2 ± 8.0	
245 4478.610 86	15.9 ± 8.0	
245 4478.666 96	−4.3 ± 8.0	
245 4478.757 02	−15.9 ± 8.0	
245 4479.645 73	−39.8 ± 8.0	
245 4479.651 26	−26.7 ± 8.0	
245 4479.702 77	−21.2 ± 8.0	
245 4479.707 22	−44.8 ± 8.0	
245 4479.711 59	−31.9 ± 8.0	
245 4479.769 92	−37.1 ± 8.0	
245 4479.730 92	−26.5 ± 8.0	
245 4479.780 20	−34.4 ± 8.0	
245 5211.024 31	−11.5 ± 0.6	UCLES
245 5499.759 01	−12.1 ± 0.2	FEROS
245 5501.636 76	31.1 ± 0.3	
245 5501.643 80	31.0 ± 0.3	
245 5501.656 52	29.7 ± 0.3	
245 5501.823 39	15.4 ± 0.2	
245 5501.832 16	14.9 ± 0.2	

Six additional high-resolution spectra have been taken with Fiber-fed Extended Range Optical Spectrograph (FEROS) ($R \simeq 48000$, λ = 3750–9200 Å) mounted at the ESO Max-Planck-Institut Garching (MPG) 2.2-m telescope in 2010 October/November.

The RVs were measured with high accuracy from sharp, unblended metal and helium lines by fitting functions with the Bamberg Spectrum Plotting and Analysis Suite (SPAS; Hirsch 2009). The UCLES spectra were co-added and the RV determined in the same way. The RV measurements are given in Table 1.

3 ORBITAL SOLUTION

In order to derive the orbital solution, sine curves were fitted to the RV data points in fine steps over a range of test periods. For each period the χ^2 of the best-fitting sine curve was determined. The lowest χ^2 indicates the most likely period. The orbital parameters are given in Table 2.

We performed a Monte Carlo simulation for the most likely periods. For each of the 10 000 iterations, a randomized set of RVs was drawn from Gaussian distributions with central value and width corresponding to the RV measurements and the analysis repeated (see Fig. 1). The probability that the solution with the lowest χ^2 and $P = 2.3098 \pm 0.0003$ d is the correct one is estimated to be 96 per cent. The reduced χ^2 of this solution is ≃1.3. The second best alias

Table 2. Orbital parameters of CPD−20°1123.

T_0 (HJD)	245 5500.86 ± 0.01
P	2.3098 ± 0.0003 d
γ	−6.3 ± 1.2 km s^{-1}
K	43.5 ± 0.9 km s^{-1}
$f(M)$	0.019 M$_\odot$
$M_{\rm sdB}$ (adopted)	0.47 M$_\odot$
$M_{2,\rm min}$	0.21 M$_\odot$

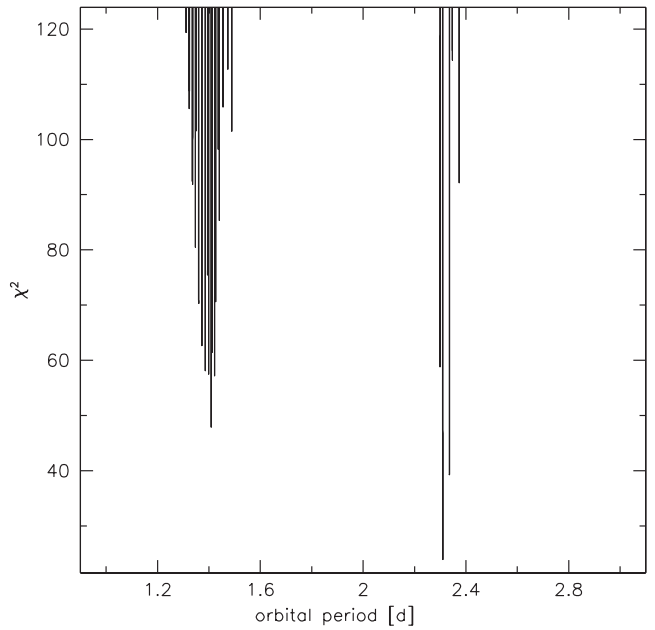

Figure 1. χ^2 of the best sine fit is plotted against the orbital period. Minima represent likely orbital periods.

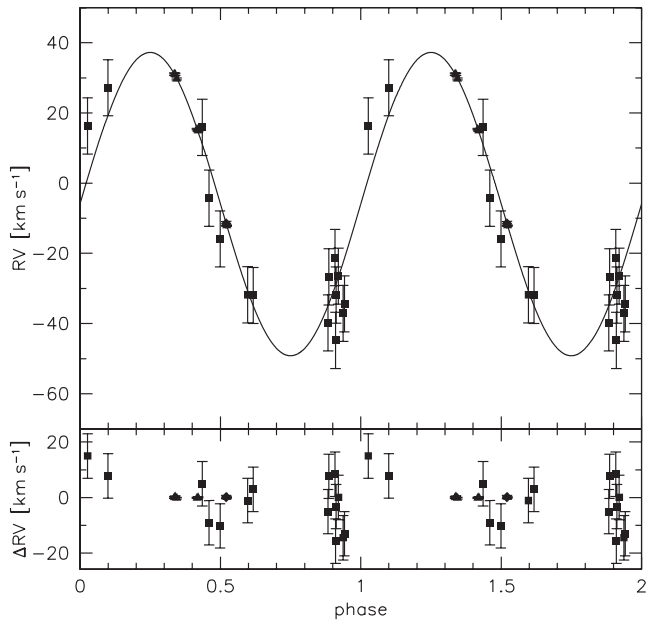

Figure 2. RVs of the subdwarf plotted against orbital phase. The residuals are plotted below. Filled rectangles mark RVs measured from EMMI spectra, filled triangles mark RVs obtained from FEROS spectra and the filled diamond marks the RV measured from the co-added UCLES spectrum.

period ($P = 2.3361$ d) with $\Delta\chi^2 = 15$ has a probability of 0.8 per cent to be the correct one (see Fig. 1).

In order to derive conservative errors for the RV semi-amplitude K and the system velocity γ we fixed the most likely period, created new RV data sets with a bootstrapping algorithm and calculated the orbital solutions. The standard deviation of these results was adopted as error estimate and is about twice as high as the 1σ error. The phase-folded RV curve is shown in Fig. 2, while the orbital parameters are given in Table 2.

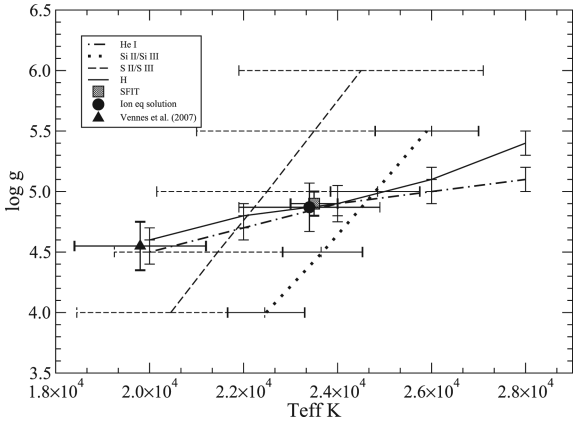

Figure 3. The loci of ionization equilibria for Si II/III and S II/III, the profile fits to H and He I lines and the adopted solution for CPD−20°1123.

Adopting the frequently assumed sdB mass of $0.47\,M_\odot$, the minimum mass of the companion ($0.21\,M_\odot$) can be derived from the binary mass function. No spectral features of the companion are visible. The unseen object could be a late main-sequence star with a mass ranging from 0.21 to $\simeq 0.45\,M_\odot$. A more massive main-sequence star would contribute sufficient light to be visible in the spectrum. The companion may also be a white dwarf. In this case its mass would be less well constrained.

Owing to the long orbital period of CPD−20°1123, it is hardly possible to detect the reflection effect due to a cool M dwarf companion with ground-based photometry. Koen (2009) detected the reflection effect with an amplitude of 10 mmag in the sdB+M dwarf binary JL 82. JL 82 has an orbital period of 0.75 d, making it the longest period sdB binary in which this effect has been observed. With an orbital period three times longer, CPD−20°1123 would exhibit a reflection-effect amplitude of a few mmag at most. Whilst such signals are detectable if the periods are sufficiently short (i.e. hours), they are almost impossible to detect if the periods are of the order of days.

4 ATMOSPHERIC PARAMETERS

We measured the effective temperature $T_{\rm eff}$, surface gravity $\log g$ and elemental abundances of CPD−20°1123 using the method described by Naslim et al. (2010). The microturbulent velocity determined by minimizing the scatter in the nitrogen abundance was $v_{\rm t} = 9 \pm 3\,{\rm km\,s^{-1}}$. Since no model atmospheres with $v_{\rm t} = 9\,{\rm km\,s^{-1}}$ were readily available, those with $v_{\rm t} = 10\,{\rm km\,s^{-1}}$ were used in the subsequent formal solution for the ionization equilibria and the abundance measurements. We determined $T_{\rm eff}$ using the ionization equilibria of Si II/III and S II/III. The surface gravity $\log g$ was determined by using line-profile fits to the Stark-broadened He I 4471 and Balmer (H_β, γ and δ) lines. The coincidence of profile fits and ionization equilibria was used to determine the overall solution shown in Fig. 3. The ionization equilibria and profile fits do not

Table 3. Atmospheric parameters of CPD−20°1123.

$T_{\rm eff}$(K)	$\log g$	$n_{\rm He}$	Source
23 500 ± 500	4.9 ± 0.1	0.170 ± 0.05	SFIT
23 400 ± 1 500	4.87 ± 0.2		Ion eq
19 800 ± 1 400	4.55 ± 0.2	0.150 ± 0.15	Vennes et al. (2007)

Table 4. Individual line equivalent widths W_λ and abundances ϵ_i, with adopted oscillator strengths gf, for CPD−20°1123.

Ion λ (Å)	log gf	W_λ (mÅ)	ϵ_i
C II			
4267.02	0.559⌉	58	6.71
4267.27	0.734⌋		
N II			
3995.00	0.225	116	7.89
4041.31	0.830	80	8.07
4043.53	0.714	65	8.03
4236.86	0.396⌉	85	8.19
4236.98	0.567⌋		
4241.78	0.728⌉	72	8.19
4241.79	0.710⌋		
4447.03	0.238	75	8.08
4601.48	−0.385	85	8.34
4607.16	−0.483	71	8.29
4630.54	0.093	110	8.11
4056.90	−0.461	32	8.76
4073.05	−0.160	42	8.61
4171.59	0.281	32	8.06
4176.16	0.600	53	8.05
4530.40	0.671	51	8.12
4643.09	−0.385	70	8.20
4613.87	−0.607	70	8.41
O II			
4649.14	0.342	26	7.53
4414.90	0.210	10	7.17
4069.88	0.365⌉	12	7.26
4069.62	0.158⌋		
4075.86	0.700	21	7.47
4416.97	−0.041	20	7.78
Mg II			
4481.13	0.568⌉	137	6.92
4481.33	0.732⌋		
Al III			
4512.54	0.405	45	6.26
4529.20	0.660	55	6.12
4479.97	1.021⌉	43	6.44
4479.89	0.894⌋		
4149.90	0.619⌉	43	6.29
4150.14	0.464⌋		
Si II			
4128.07	0.369	50	6.90
4130.89	0.545	51	6.73
Si III			
4552.62	0.283	111	6.96
4567.82	0.061	85	6.96
4574.76	−0.416	60	7.17
P III			
4059.31	−0.050	22	5.62
4222.19	0.190	40	5.74
S II			
4815.52	−0.050	47	7.44
4716.23	−0.050	22	7.50
4524.95	0.061	25	7.36
4294.43	0.560	30	7.20
4162.70	0.785	33	6.97
4153.10	0.681	33	7.08
S III			
4253.59	0.233	36	6.72
4284.99	−0.046	30	7.03
Cl II			
4794.54	0.423	31	6.38
4810.06	0.281	25	6.43
4896.74	0.450	28	6.96[a]
Ar II			
4401.02	−0.250	16	6.91
4371.36	−0.570	25	7.44
4806.07	0.215	37	6.97
4879.90	0.220	24	6.88
4426.01	0.170	26	6.82
4609.60	0.286	21	7.05
4726.91	−0.180	15	7.03
4735.93	−0.108	24	7.06
4764.89	−0.110	15	7.00
4657.90	−0.283	14	7.10
Fe III			
4164.73	0.935	24	7.13
4166.84	0.436	15	7.38
4419.60	−2.218	20	7.16
4395.76	−2.595	12	7.30
4166.86	0.436	15	7.38

gf values: C II (Yan, Taylor & Seaton 1987); N II (Becker & Butler 1989); O II (Becker & Butler 1988); Mg II (Wiese, Smith & Glennon 1966); Al III (Canuto & Mendoza 1969; McEachran & Cohen 1983); Si II (Becker & Butler 1990); Si III (Becker & Butler 1990); P III (Wiese, Smith & Miles 1969); S II (Wiese et al. 1969); S III (Wiese et al. 1969; Hardorp & Scholz 1970); Cl II (Rodriguez & Campos 1989); Ar II (Wiese et al. 1969); Fe III (Kurucz 1991).

[a]Line abundance omitted from mean in Table 5.

coincide at a single point so that we took a weighted mean of the intersections to determine $T_{\rm eff}$ and $\log g$.

In addition, the χ^2-minimization package SFIT (Ahmad & Jeffery 2003) was used to determine $T_{\rm eff}$, $\log g$ and $n_{\rm He}$ simultaneously. Initially we selected an assumed model atmosphere grid with 1/10 solar metallicity as well as solar metallicity with $T_{\rm eff} = 18\,000$ (2000) 28 000 K, $\log g = 4.00(0.5)5.50$ and $n_{\rm He} = 0.2,\ 0.3$ and 0.5. We adopted a microturbulent velocity of $10\,{\rm km\,s^{-1}}$. Using SFIT we obtained a reduced χ^2 fit for model with 1/10 solar metallicity and $n_{\rm He} = 0.2$. A model atmosphere grid of $T_{\rm eff} = 20\,000$ (2000) 26 000 K, $\log g = 4.00\,(0.5)\,5.50$ and $n_{\rm He} = 0.1, 0.2$ and 0.3 was used to determine the best-fitting solution. The projected rotational velocity obtained from the formal solution was $v \sin i \leq 1.0 \pm 0.5\,{\rm km\,s^{-1}}$; the true value may be slightly larger.

The atmospheric parameters of CPD−20°1123 measured using both SFIT and ionization equilibrium agree with one another to

Table 5. Mean abundances ϵ_i for CPD−20°1123.

El.	CPD−20°1123	sdB[a,b,c,d,e]	JL 87[f]	LS IV−14°116[g]	He-sdB[h]	Sun[i]
H	11.85 ± 0.1	12.0	11.6	11.83	<8.5–11.1	12.00
He	11.17 ± 0.1	7.9–11.0	11.3	11.15	11.5	[10.93]
C	6.71 ± 0.1	5.5–9.5	8.8	8.04	6.5–9.0	8.52
N	8.21 ± 0.21	6.5–8.5	8.8	8.02	8.0–9.0	7.92
O	7.41 ± 0.23	6.0–8.5	8.6	7.60	6.8–7.5	8.83
Ne	<7.5	6.5–8.5	8.31	<7.6	7.7–9.0	[8.08]
Mg	6.92 ± 0.10	5.5–7.8	7.4	6.85	7.0–8.5	7.58
Al	6.31 ± 0.13	4.5–7.0	6.3		6.0–6.4	6.47
Si	6.94 ± 0.16	5.0–7.7	7.2	6.32	6.5–7.5	7.55
P	5.68 ± 0.10	4.5–6.0	5.3			5.45
S	7.09 ± 0.28	5.0–8.0	6.9		6.0–7.0	7.33
Cl	6.40 ± 0.10					5.5
Ar	7.03 ± 0.17	6.0–9.0	6.3	<6.5		[6.40]
Sc	<3.5	5.0–7.0		<5.3		3.17
Ti	<5.8	5.3–9.0		<6.0		5.02
V	<6.0	6.0–8.5		<6.5		4.00
Cr	<6.5	5.5–8.0		<7.0		5.67
Fe	7.27 ± 0.12	6.5–8.1	7.5	<6.8		7.50

References: [a]Edelmann et al. (2003); [b]Geier, Heber & Napiwotzki (2008); [c]Geier et al. (2010); [d]O'Toole & Heber (2006); [e]Chayer et al. (2006); [f]Ahmad et al. (2007); [g]Naslim et al. (2011); [h]Naslim et al. (2010); [i]Grevesse & Sauval (1998).
The solar helium abundance is the asteroseismic value for the outer convection zone, and the solar neon and argon abundances are the meteoritic values; other solar abundances are for the solar photosphere.

within the formal errors and are shown in Table 3. Our estimates of $T_{\rm eff}$ and $\log g$ are different from the measurements by Vennes et al. (2007). The latter used an intermediate-resolution optical spectrum and line-blanketed non-local thermodynamic equilibrium (NLTE) model atmospheres for their analysis. They determined $T_{\rm eff}$, $\log g$ and $n_{\rm He}$ from the Balmer and He I line fitting. The atmospheric parameters presented here were determined from Balmer and He I line fitting, Si II/III and S II/III ionization equilibria. The reason for the discrepancy might be the use of two different methods of analyses. It is noted that Si II/III and S II/III ionization temperatures match better the Balmer and He I lines at higher $T_{\rm eff}$ and $\log g$ (Fig. 3).

5 ABUNDANCES

For abundance measurements the model atmosphere with $T_{\rm eff} = 24\,000$ K, $\log g = 5.0$, $n_{\rm He} = 0.2$ and 1/10 solar metallicity was adopted. After measuring the equivalent widths of all C, N, O, Mg, Al, Si, S, Cl, Ar and Fe lines using the spectrum analysis tool DIPSO, the abundances were calculated using the LTE radiative transfer code SPECTRUM (Jeffery, Woolf & Pollacco 2001). The adopted oscillator strengths (gf), equivalent widths and lines abundances are given in Table 4. Abundances are given in the form $\epsilon_i = \log n_i + c$. where $\log \Sigma_i a_i n_i = 12.15$ and a_i are atomic weights. This form conserves values of ϵ_i for elements whose abundances do not change, even when the mean atomic mass of the mixture changes substantially.

Mean abundances for each element are given in Table 5. The errors given in Table 5 are based on the standard deviation of the line abundances about the mean or in the case of a single representative line, the estimated error in the equivalent width measurement. Systematic shifts attributable to errors in $T_{\rm eff}$ and $\log g$ are given in Table 6. The line abundance for Cl II 4896.7 Å is conservatively omitted from the mean since the high abundance implied is not supported by the non-detection of Cl II 4904.7 Å.

Table 6. Systematic abundance errors $\delta\epsilon_i$ due to representative errors in $T_{\rm eff}$ and $\log g$.

Element	$\delta T_{\rm eff} = 1000$ K	$\delta \log g = 0.2$
C	0.05	−0.03
N	0.15	−0.06
O	0.18	−0.08
Mg	−0.09	0.03
Al	0.11	−0.05
Si	0.05	−0.04
P	0.11	−0.08
S	0.05	−0.04
Cl	−0.20	0.05
Ar	0.005	−0.02
Fe	0.11	−0.08

The final best-fitting spectrum using the adopted best-fitting model and the elemental abundances from Table 5 is shown in Fig. 4, together with identifications for all of the absorption lines in the model. The elemental abundances shown in Table 5 are the mean abundances of all individual lines of an ion. Consequently, the cores of strong and saturated lines do not fit perfectly in Fig. 4. A few features on the observed spectrum (e.g. 4423.93 Å) are not explained by the model, but might be defects from the order merging process.

Table 5 also compares the representative range of abundances measured for normal sdB stars, for intermediate helium sdB stars JL 87 and LS IV−14°116, for extreme helium rich sdB stars and the Sun. CPD−20°1123 appears to be metal poor (≈0.5 ± 0.3) using magnesium, aluminium, silicon, sulphur and iron as proxies for overall metallicity. The nitrogen abundance is nearly solar and carbon is underabundant by ≈1.8 dex. This star shows strong argon and chlorine enrichment (≈0.63 and 0.9 dex, respectively). The iron group elements Sc, Ti, V, Cr and Fe have been reported in certain

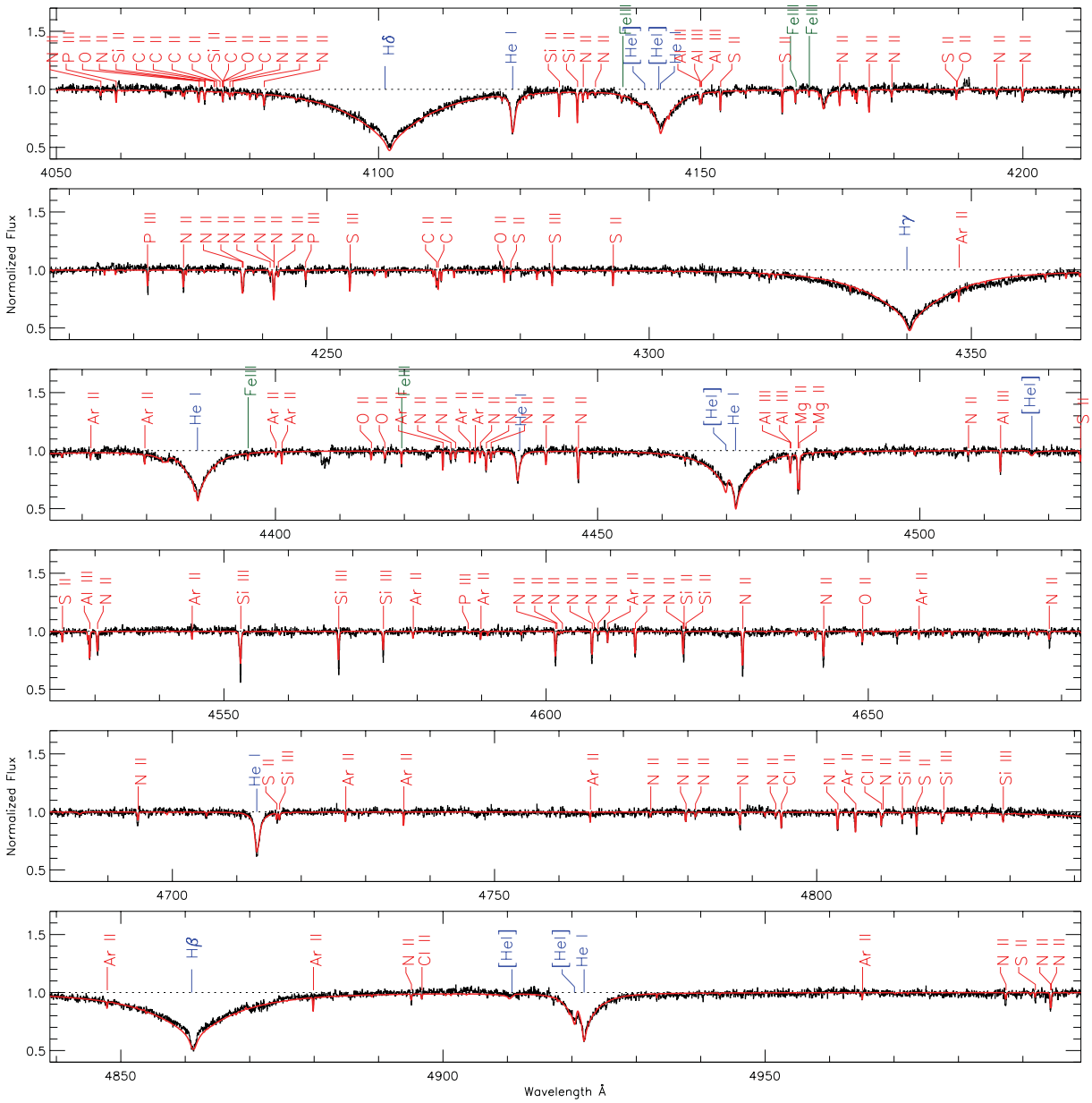

Figure 4. The merged AAT/UCLES spectrum of CPD−20°1123 along with the best-fitting model of $T_{\rm eff} = 24\,000$ K and $\log g = 5.0$. Abundances are as in Table 5.

normal sdB stars (O'Toole & Heber 2006; Geier et al. 2008, 2010). The iron abundance in CPD−20°1123 is found to be subsolar, and no detectable lines due to Sc, Ti, V and Cr were identified in the optical spectrum. The upper limit abundances of these elements were determined, assuming equivalent widths <5 mÅ for the strongest lines of these species (Table 5). More lines due to Fe and other iron group elements should be observable in the ultraviolet. The UCLES data used for this analysis are insufficient to search for variability.

6 IS CPD−20°1123 A HELIUM-RICH STAR?

CPD−20°1123 attracted attention because it appears to be a bright sdB star with unusually strong helium lines (Vennes et al. 2007). Indeed, a fine analysis demonstrates the helium abundance to be nearly a factor of 2 greater than solar. This places CPD−20°1123 firmly amongst the intermediate helium rich sdB stars alongside JL 87, LS IV−14°116 and others. A *normal* sdB star tends to have helium abundances 2 or 3 dex below solar.

The question raised by the intermediate helium rich sdB stars is how or whether they are related to normal sdB stars or to the extremely helium rich sdB stars or to neither. One is tempted to distinguish the extremely helium rich and normal sdB stars on the basis of position in the g–$T_{\rm eff}$ diagram (Fig. 5) as well as surface composition. Zhang & Jeffery (2012) argue strongly that the former are post-double-white dwarf mergers evolving on to the helium main sequence, with surface chemistries dominated by the constituents of the merger.

The intermediate helium rich sdB stars, on the other hand, lie much closer to the locus of the normal sdB stars although also towards the low-gravity boundary. It is important to remember that the surface chemistry of normal sdB stars is dominated by diffusion activated by strong gradients in the radiative forces acting on

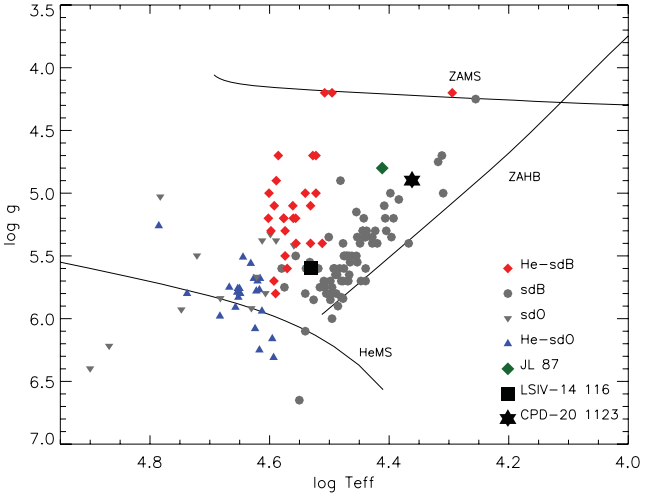

Figure 5. The location of CPD−20°1123 on the log g–$T_{\rm eff}$ diagram, compared with normal sdB stars (Edelmann et al. 2003), helium-rich sdB stars (Ahmad & Jeffery 2003; Naslim et al. 2010), helium-rich sdO stars (Stroeer et al. 2007), LS IV−14°116 (Naslim et al. 2011) and JL 87 (Ahmad et al. 2007). A zero-age main sequence ($Y = 0.28$, $Z = 0.02$), a zero-age horizontal branch ($M_{\rm c} = 0.485{\rm M}_{\odot}$, $Y_{\rm e} = 0.28$, $Z = 0.02$) and a helium main sequence ($Z = 0.02$) are also shown.

different elements. The chemical separation induced by these gradients does not occur instantaneously but takes some 10^5–10^6 yr, a small but finite fraction of the lifetime of an extended horizontal branch star (10^8 yr).

What is the surface chemistry of an sdB star progenitor? Clearly, the answer depends on what sort of star the progenitor was. Excluding double-white dwarf mergers, current understanding indicates the most likely possibilities are helium-core red giants (Dorman, Rood & O'Connell 1993) who lose their outer layers either by a fast stellar wind (D'Cruz et al. 1996), by stable Roche lobe overflow (Green, Liebert & Saffer 2000) or by common-envelope ejection (Han et al. 2002). As a consequence of first dredge-up on the first giant branch, it is expected that the surface layers of the red giant will have above-solar abundances of helium and nitrogen. Since less than $0.002\,{\rm M}_{\odot}$ of hydrogen-rich material survives the mass-loss episode, which is less than the natural thickness of the hydrogen-burning shell in a red giant, these remaining layers may or may not be deep enough to have been further enriched in helium. Following core-helium ignition, the surviving star contracts on to the extended horizontal branch by one of several routes (Lanz et al. 2004; Miller Bertolami et al. 2008; Miller Bertolami, Córsico & Althaus 2011) on a time-scale of $\approx 10^6$ yr.

Once the surface temperature exceeds some 10 000 K and the surface gravity approaches some $10\,000\,{\rm cm\,s^{-2}}$, radiatively driven diffusion becomes effective, and ultimately the helium and other light elements sink beneath the hydrogen. During this process, it is not inconceivable that the outer layers of the star become heavily stratified, with elements being concentrated at depths where their specific opacities are high. Such appears to be the case for the extraordinary 'zirconium star' LS IV−14°116. Such exotic mixtures may simply be a precursor to that which is referred to as normal for an sdB star.

Now it is well established that some 50–70 per cent (at least) of normal sdB stars are members of binary systems (Maxted et al. 2001; Geier et al. 2011). If intermediate helium rich sdB stars are simply the precursors of normal sdB stars, then the fraction of both groups which are binaries should be the same. Until now, an argument against the precursor hypothesis was that no intermediate helium star was known to be a binary. However, such an argument only has merit with the inclusion of UVO 0512−08 and PG 0909+276 (Edelmann 2003) in addition to LS IV−14°116 (Naslim et al. 2011) and JL 87 (Ahmad et al. 2007). The discovery that CPD−20°1123 is a short-period binary with a probable white dwarf or a late main-sequence companion reverses the argument and supports the possibility that intermediate helium rich and normal sdB stars derive from a similar group of progenitors. We note this is *not* the same as saying that one type evolves into the other.

Two additional facts may be important.

(i) All known intermediate helium rich sdB stars[1] have very small projected rotation velocities ($v \sin i$). A similar result has been found for normal sdB stars which are *not* in close binaries with periods less than ≈1.2 d (Geier et al. 2012). Slow rotation is believed to be a necessary condition contributing to chemical peculiarity in mercury–manganese stars (Wolff & Preston 1978). Fast rotation may cause mixing effects which prevent elements from being concentrated in stratified layers.

(ii) CPD−20°1123 lies at the cool end of the sdB domain. The diffusion time-scale should be longer at lower $T_{\rm eff}$ and g, so that peculiar surface chemistries may be relatively more likely. It would be interesting to look for more helium-strong sdB stars at the cool end of the sdB sequence.

7 CONCLUSION

With a helium abundance about twice solar, CPD−20°1123 is securely determined to be an intermediate helium rich subdwarf B star. Chemically these are quite distinct from normal sdB stars (which are helium poor) and extremely helium rich sdB stars (more than 80 per cent helium). The abundances of other elements in CPD−20°1123 are slightly peculiar; high argon and chlorine, and detectable iron are noted in particular.

CPD−20°1123 is the first intermediate helium rich sdB star found to be a short-period binary. With a period of 2.3 d, the companion could be either a low-mass main-sequence star or a white dwarf.

It is argued that a high helium abundance would be expected for the surface of a very young sdB star, evolving from the tip of the first red giant branch after having lost its hydrogen-rich envelope. This helium will sink out of sight within the first 10^6 yr of evolution on the extended horizontal branch. It is proposed that the intermediate helium sdB stars are simply very young normal sdB stars in which this process has yet to be completed.

It is expected that as the number of known intermediate helium sdB stars increases, the number found to be members of binaries will also increase, as will the variety of their surface chemistries. Understanding how the surface chemistries of these stars change is a challenge for both theory and observation but will ultimately help explain how sdB stars are formed.

ACKNOWLEDGMENTS

This paper is based on observations obtained with the Australian Astronomical Telescope and on observations at the La Silla Observatory of the European Southern Observatory for programmes number 080.D-0685(A) and 086.D-0714(A).

The Armagh Observatory is funded by direct grant from the Northern Ireland Dept of Culture Arts and Leisure. S. G. is

[1] JL 87, LS IV−14°116, UVO 0512–08, PG 0909+276 and CPD−20°1123.

supported by the Deutsche Forschungsgemeinschaft under grant HE1356/49-1.

REFERENCES

Ahmad A., Jeffery C. S., 2003, A&A, 402, 335
Ahmad A., Jeffery C. S., 2004, Ap&SS, 291, 253
Ahmad A., Jeffery C. S., 2006, Baltic Astron., 15, 139
Ahmad A., Behara N. T., Jeffery C. S., Sahin T., Woolf V. M., 2007, A&A, 465, 541
Becker S. R., Butler K., 1988, A&A, 209, 244
Becker S. R., Butler K., 1989, A&A, 235, 326
Becker S. R., Butler K., 1990, A&A, 201, 232
Caballero J. A., Solano E., 2007, ApJ, 665, L151
Canuto W., Mendoza C., 1969, Rev. Mex. Astron. Astrofis, 23, 107
Chayer P., Fontaine M., Fontaine G., Wesemael F., Dupuis J., 2006, Baltic Astron., 15, 131
D'Cruz N. L., Dorman B., Rood R. T., O'Connell R. W., 1996, ApJ, 466, 359
Dorman B., Rood R. T., O'Connell R. W., 1993, ApJ, 419, 596
Edelmann H., 2003, PhD thesis, Friedrich-Alexander Universität Erlangen-Nürnberg
Edelmann H., Heber U., Hagen H., Lemke M., Dreizler S., Napiwotzki R., Engels D., 2003, A&A, 400, 939
Geier S., Heber U., Napiwotzki R., 2008, in Heber U., Jeffery C. S., Napiwotzki R., eds, ASP Conf. Ser. Vol. 392, Hot Subdwarf Stars and Related Objects. Astron. Soc. Pac., San Francisco, p. 159
Geier S., Heber U., Edelmann H., Morales-Rueda L., Napiwotzki R., 2010, Ap&SS, 329, 127
Geier S. et al., 2011, A&A, 530, A28
Geier S., Edelmann H., Napiwotzki R., Morales-Rueda L., 2012, in ASP Conf. Ser. Vol. 452, Fifth Meeting on Hot Subdwarf Stars and Related Objects. Astron. Soc. Pac., San Francisco, p. 81
Gill D., Kapteyn J. C., 1896, Ann. Cape Obser., 3, 1
Green R. F., Schmidt M., Liebert J., 1986, ApJS, 61, 305
Green E. M., Liebert J., Saffer R. A., 2000, BAAS, 32, 1477
Grevesse N., Sauval A. J., 1998, Space Sci. Rev., 85, 161
Han Z., Podsiadlowski P., Maxted P. F. L., Marsh T. R., Ivanova N., 2002, MNRAS, 336, 449
Hardorp J., Scholz M., 1970, ApJS, 19, 193
Heber U., 1986, A&A, 155, 33
Hirsch H., 2009, PhD thesis, Universität Erlangen-Nürnberg
Jeffery C. S., Woolf V. M., Pollacco D. L., 2001, A&A, 376, 497
Koen C., 2009, MNRAS, 395, 979
Kurucz R. L., 1991, in Philip A. G. D., Upgren A. R., Janes K. A., eds, Precision Photometry: Astrophysics of the Galaxy. Davis Press, Schenectady, NY, p. 27
Lanz T., Brown T. M., Sweigart A. V., Hubeny I., Landsman W. B., 2004, ApJ, 602, 342
McEachran R., Cohen M., 1983, J. Phys. B, 16, 3125
Maxted P. f. L., Heber U., Marsh T. R., North R. C., 2001, MNRAS, 326, 1391
Miller Bertolami M. M., Althaus L. G., Unglaub K., Weiss A., 2008, A&A, 491, 253
Miller Bertolami M. M., Córsico A. H., Althaus L. G., 2011, ApJ, 741, L3
Moehler S., Richtler T., de Boer K. S., Dettmar R. J., Heber U., 1990, A&AS, 86, 53
Napiwotzki R. et al., 2004, in Hilditch R. W., Hensberge H., Pavlovski K., eds, ASP Conf. Ser. Vol. 318, Spectroscopically and Spatially Resolving the Components of the Close Binary Stars. Astron. Soc. Pac., San Francisco, p. 402
Naslim N., Jeffery C. S., Ahmad A., Behara N. T., Şahìn T., 2010, MNRAS, 409, 582
Naslim N., Jeffery C. S., Behara N. T., Hibbert A., 2011, MNRAS, 412, 363
O'Toole S. J., Heber U., 2006, A&A, 452, 579
Rodriguez L. F., Campos J., 1989, J. Quant. Spectrosc. Radiative Transfer, 41, 377
Stroeer A., Heber U., Lisker T., Napiwotzki R., Dreizler S., Christlieb N., Reimers D., 2007, A&A, 462, 269
Vennes S., Kawka A., Smith J. A., 2007, ApJ, 668, L59
Wiese W., Smith M., Glennon, 1966, Atomic Transition Probabilities Vol. 1, Hydrogen Through Neon. A Critical Data Compilation. National Bureau of Standards, US Department of Commerce, Washington, D. C.
Wiese W., Smith M., Miles B., 1969, Atomic Transition Probabilities Vol. 2, Sodium Through Calcium. A Critical Data Compilation, National Bureau of Standards, US Department of Commerce, Washington, D. C.
Wolff S. C., Preston G. W., 1978, ApJS, 37, 371
Yan C., Taylor K., Seaton M., 1987, J. Phys. B, 20, 6399
Zhang X., Jeffery C. S., 2012, MNRAS, 419, 452

This paper has been typeset from a TEX/LATEX file prepared by the author.